





RESEARCH ARTICLE | NOVEMBER 12 2019

Enhanced piezoresponse and nonlinear optical properties of fluorinated self-assembled peptide nanotubes

Special Collection: [2019 Nanoscience and Nanotechnology](#)

Soma Khanra; Sandra V. Vassiliades; Wendel A. Alves ; Kaidi Yang; Rainer Glaser; Kartik Ghosh; Payal Bhattacharya; Ping Yu ; Suchismita Guha  



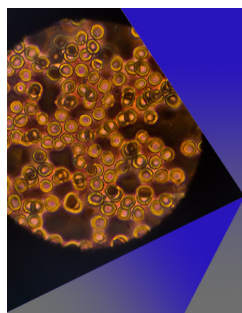
AIP Advances 9, 115202 (2019)

<https://doi.org/10.1063/1.5110562>

 CHORUS



CrossMark



AIP Advances

Special Topic: Medical Applications of Nanoscience and Nanotechnology

Submit Today!



Enhanced piezoresponse and nonlinear optical properties of fluorinated self-assembled peptide nanotubes

Cite as: AIP Advances 9, 115202 (2019); doi: 10.1063/1.5110562

Submitted: 18 May 2019 • Accepted: 29 October 2019 •

Published Online: 12 November 2019



View Online



Export Citation



CrossMark

Soma Khanra,¹ Sandra V. Vassiliades,² Wendel A. Alves,²  Kaidi Yang,³ Rainer Glaser,^{3,4} Kartik Ghosh,⁵ Payal Bhattacharya,¹ Ping Yu,¹  and Suchismita Guha^{1,a)} 

AFFILIATIONS

¹Department of Physics and Astronomy, University of Missouri, Columbia, Missouri 65211, USA

²Centro de Ciências Naturais e Humanas, Universidade Federal do ABC, 09219-580 Santo André, São Paulo, Brazil

³Department of Chemistry, University of Missouri, Columbia, Missouri 65211, USA

⁴Missouri University of Science and Technology, Rolla, Missouri 65409, USA

⁵Physics, Astronomy, and Materials Science, Missouri State University, Springfield, Missouri 65897, USA

^{a)} Author to whom correspondence should be addressed: guhas@missouri.edu

ABSTRACT

Self-assembled *L,L*-diphenylalanine (FF) nanostructures offer an attractive platform for photonics and nonlinear optics. The nonlinear optical (NLO) coefficients of FF nanotubes depend on the diameter of the tube [S. Khanra *et al.* Phys. Chem. Chem. Phys. **19**(4), 3084–3093 (2017)]. To further enhance the NLO properties of FF, we search for structural modifications. Here, we report on the synthesis of fluorinated FF dipeptides by replacing one ortho-hydrogen atom in each of the phenyl groups of FF by a fluorine atom. Density-functional theoretical calculations yield insights into minimum energy conformers of fluorinated FF (FI-FF). FI-FF self-assembles akin to FF into micron-length tubes. The effects of fluorination are evaluated on the piezoelectric response and nonlinear optical properties. The piezoelectric d_{15} coefficient of FI-FF is found to be more than 10 times higher than that of FF nanotubes, and the intensity of second harmonic generation (SHG) polarimetry from individual FI-FF nanotubes is more than 20 times that of individual FF nanotubes. Furthermore, we obtain SHG images to compare the intensities of FF and FI-FF tubes. This work demonstrates the potential of fluorine substitution in other self-assembled biomimetic peptides for enhancing nonlinear optical response and piezoelectricity.

© 2019 Author(s). All article content, except where otherwise noted, is licensed under a Creative Commons Attribution (CC BY) license (<http://creativecommons.org/licenses/by/4.0/>). <https://doi.org/10.1063/1.5110562>

Nonlinear optical (NLO) phenomena are fundamental to important technological tools in optoelectronics. Proteins are a class of structurally and functionally diverse biopolymers, which are intrinsically chiral, and collagens, muscle tissue, and fibrillar proteins are known to show NLO properties.^{1–3} Second harmonic generation (SHG) occurs in materials that do not possess inversion symmetry. In general, a large number of bioinspired materials have noncentrosymmetric crystal structures,⁴ and self-assembly of these materials results in hollow tubes which are suitable to measure SHG⁵ and optical wave-guiding.^{6–8} To improve these materials systematically requires the development of structure-function relationships and attempts to modify the optical properties of the

biomaterials without jeopardizing their polar superstructures. *L,L*-diphenylalanine (FF, more correctly named as *L*-phenylalanyl-*L*-phenylalanine) is one prominent dipeptide which has been studied extensively (*vide infra*). We report here on the design and synthesis of a fluorinated derivative FI-FF (correctly named as 2-fluoro-*L*-phenylalanyl-2-fluoro-*L*-phenylalanine) which is informed by the analysis of the superstructure of FF. Using similar methods for materials fabrication and characterization,⁹ we demonstrate that the properties of the fluorinated material, FI-FF, greatly exceed those of the parent FF material.

Since the discovery of self-assembly in FF, extensive studies have been carried out to characterize its mechanical rigidity,¹⁰

chemical and thermal stabilities,^{11,12} nonreversible phase transition,¹² wave guiding,¹³ and chiroptical activity.^{14,15} Self-assembled FF microstructures/nanostructures have been utilized in various applications such as biosensing,^{16–18} drug delivery,¹⁹ mechanical reinforcement,^{19,20} energy generation,^{21,22} organic electronics,^{23,24} and photodynamic therapy.²⁵ The nonlinear optical properties of as-synthesized FF nanotubes are attributed to the material's $P6_1$ noncentrosymmetric space group,¹² which further gives rise to ferroelectricity^{26–28} and piezoelectricity.²⁹

A key question concerns possibilities for chemical modifications of FF which may allow for an enhancement of the SHG and piezoelectric responses while still maintaining the self-assembly process. Such an approach may substantially advance the area of nanophotonics and open a new realm of self-assembled photonic

metamaterials. In this work, we take a cue from fluorinated polymers, where the outstanding piezoelectric and ferroelectric properties of polyvinylidene fluoride (PVDF) have stimulated numerous studies over five decades.^{30–32} The introduction of the copolymer poly(vinylidene fluoride-co-trifluoroethylene), P(VDF-TrFE), where one methylene-H atom is replaced by F in the TrFE unit, results in a strong ferroelectric response due to the all-*trans* conformation.³³ The difference in bond dipole moments of the C–H and C–F bonds on opposite sides of the polymer chain leads to a large dipole moment. In these cases, the fluorine atom is both part of the NLO chromophore and also directly responsible for the polar alignment of the polymer chains.

Here, self-assembled FI-FF nanotubes are fabricated using the liquid vapor phase method in analogy to the self-assembly process

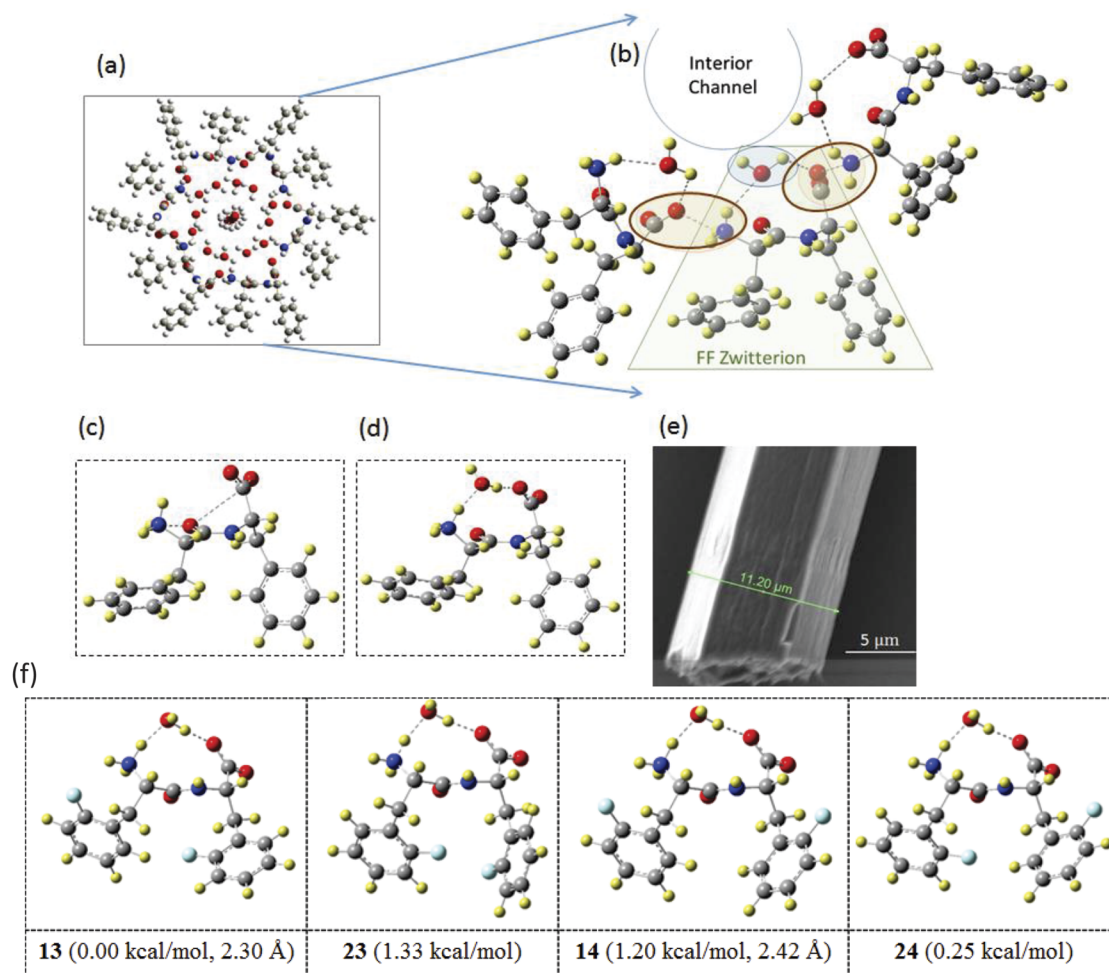


FIG. 1. (a) Chemical structure of a FF macrocycle with water molecules in the core. (b) A segment of the FF macrocycle with one FF zwitterion highlighted by the green shading. (c) The SMD(B3LYP/6-31G*) optimized structure of FF zwitterion contains a “frustrated Lewis pair” consisting of a Lewis acid (ammonium group) and a Lewis base (carboxylate) functionality. (d) The SMD(B3LYP/6-31G*) optimized structure of FF zwitterion with a water molecule bridging between the Lewis acid and Lewis base functionalities. (e) SEM image of a self-assembled FF tube. (f) Molecular models of water-bridged FI-FF zwitterion determined at the SMD(B3LYP/6-31G*) level for aqueous solution. The row below the figures contains the following information: number of the conformer (energy relative to the most stable structure and distance between the F atom and the proximate ammonium-H atom in Å).

of FF nanotubes.⁹ Detailed SHG polarimetry from FF nanotubes was conducted in Ref. 9, which forms the basis for a comparison of the nonlinear optical properties of FF and FI-FF nanotubes. The fluorination of FF in this work involves a function-based design and chemical synthesis. Individual FF and FI-FF tubes were isolated for SHG polarimetry and piezoelectric force spectroscopy.

The SHG setup is based on a Q-switched YAG:Nd³⁺ laser operating at a wavelength of 1064 nm and was configured either in the transmission geometry with a spot size of 100 μm or in a reflection geometry using a micro-SHG imaging setup. The transmission geometry was discussed in detail in Ref. 9. The SHG imaging in the reflection mode uses a long working distance 20 \times microscope objective along with a cooled EMCCD camera (Photometrics Evolve 512) for capturing images. The contact mode of the scanning probe microscope (Model: Park-NX10, Park Systems) was used to characterize the surface topography of the samples and the piezoresponse force microscopy (PFM) mode for obtaining the piezoresponse images.

The self-assembly of FF has been discussed in several articles.^{34,35} It starts with the packing of six FF dipeptides into a helical macrocycle, where the ammonium and carboxylate groups constitute the inner core of the cycle. An aqueous environment is necessary for the self-organization process, and water remains confined in the interior channel, as shown in Fig. 1(a). Theoretical calculations predict a minimum binding energy with 21 water molecules enclosed within the FF hexamer.³⁶ The elemental building block of the FF crystal is the FF zwitterion. These FF zwitterions aggregate by intermolecular interactions between positively charged ammonium moieties and negatively charged carboxylate groups, and two such ion pairing contacts are highlighted by the orange shading in Fig. 1(b). This crystal architecture results in chiral helices with six (S,S)-enantiomers of FF zwitterions per turn and allows the parallel alignment of the carbonyl groups within the amide functional groups of every one of the FF zwitterions.

Density-functional theory (DFT) calculations³⁷ employing the SMD solvation model³⁸ result in several nearly isoenergetic conformations of the benzyl moieties, and two such optimized structures calculated at the SMD(B3LYP/6-31G*) level are shown in Figs. 1(c) and 1(d). The key structural motif is the placement of the Lewis acidic ammonium group and of the Lewis basic carboxylate group in relative proximity but not close enough to form an effective Lewis pair. This “frustrated Lewis pair” motif causes the tight binding of water molecules to bridge the frustrated Lewis pair [Fig. 1(d)]. The bridging water molecule, which acts as a Lewis acid toward the FF’s Lewis base and as a Lewis base to the FF’s Lewis acid, guides the preparation of materials and serves as the basis for the design of responsive materials. An SEM image of an FF microtube/nanotube is shown in Fig. 1(e).

The NLO response of FF self-assembled tubes likely is the result of the unsymmetrical arene chromophores. In FF itself, the unsymmetrical arenes are of the type peptide-CH₂-C₆H₅, that is, they are monoalkyl substituted benzenes with the polar axis closely aligned with the C_{ipso}-C_{para} axis (C1-C4). The most obvious way to enhance the intensity of this chromophore would involve the placement of an electron-acceptor in the para-position to afford a standard donor-acceptor disubstituted benzene. However, such a modification would drastically alter the interaction between the

helical columns in the FF nanotubes. In contrast, we analyzed the crystal structure of FF in search for the positions of aromatic H atoms that could be replaced by F atoms with the least consequences for the overall crystal architecture. Hence, our focus turned to H/F replacements in the ortho position and the difluorinated FF (FI-FF) is one of the possible implementations.

Details of FI-FF synthesis and the synthesis scheme are provided in the [supplementary material](#). In FI-FF, one ortho-hydrogen atom in each of the phenyl groups of FF is replaced by a fluorine atom. In Fig. 1(f), the four conformers are shown of water-bridged FI-FF calculated at the level of SMD(B3LYP/6-31G*) for aqueous solution. The most important result becomes immediately obvious in that the structure of water-bridged FF [Fig. 1(d)] is essentially retained in all conformers of water-bridged FI-FF. In the FF structure [Fig. 1(d)], there are four ortho-positions in the two benzene rings that may be occupied by fluorine in FI-FF and we label these from left to right as 1–4 (see the synthesis scheme in the [supplementary material](#)). The names of the FI-FF conformers formally indicate the two ortho-positions that were substituted by fluorine atoms in FF. The most stable structure of FI-FF is conformer **13** (with fluorine atoms in the 1 and 3 positions of the FF structure), and the relative energies of conformers **23**, **14**, and **24** are shown in kilocalories per mole. Benzene-benzene T-contacts are observed in all of the conformers. Structures **13** and **14** benefit from hydrogen bonding between the fluorine atom in the 1-position and a proximate ammonium-H.

Figure 2 shows the electron microscopy images from FI-FF. Selected area diffraction from a high resolution transmission electron microscope image shows the crystalline nature of FI-FF [Figs. 2(a) and 2(b)]. Figures 2(c) and 2(d) show SEM images of a single FI-FF tube and multiple tubes. The lengths of the tubes may reach a couple of 100 μm .

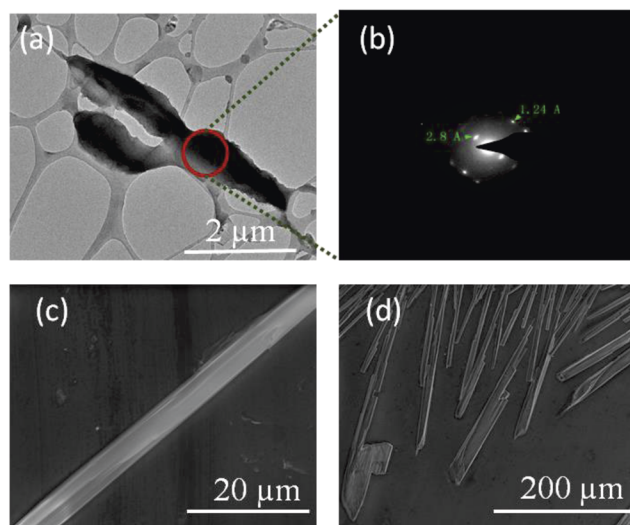


FIG. 2. (a) High-resolution transmission electron microscope image from an FI-FF nanotube. (b) Selected area electron diffraction from the highlighted area in the image in (a). SEM images of (c) a single FI-FF nanotube and (d) multiple FI-FF nanotubes.

To characterize the piezoelectric properties of the FF and FI-FF samples, we collected the PFM images as well as spectroscopy data. Since the nanotubes are on a surface, it is easier to measure the shear deformation by PFM. For optimal comparison of their piezoresponses, FF and FI-FF nanotubes with similar diameters were chosen. Figure 3 shows the PFM imaging data of FF and FI-FF nanotubes. Since the entire nanotube is piezoelectric, the piezoelectric image follows the topographical features. Details of the PFM setup are provided in the supplementary material. Figures 3(a)–3(c) show the topography, phase, and amplitude images of the FF nanotubes, and Figs. 3(d)–3(f) show the analogous images of the FI-FF nanotubes. We infer the tube diameters (outer) of both FF and FI-FF to be approximately $2\ \mu\text{m}$ from the topography images. Large phase as well as amplitude differences in the tube region compared to the nontube region clearly indicates that both tubes are piezoelectric. To compare the d_{15} value (shear response) of FF and FI-FF, piezoforce spectroscopic measurements were carried out. Figures 3(g) and 3(h) show the PFM amplitude as a function of the applied dc voltage. The background is plotted as black symbols. In both samples, the amplitude increases with voltage. The measurements were carried out such that the sample response is perpendicular to the cantilever

and, hence, our measurements yield the d_{15} component of the piezoelectric tensor. The d_{15} components, deduced from the slopes, are $50\ \text{pm/V}$ and $600\ \text{pm/V}$ for FF and FI-FF nanotubes, respectively.

Figure 4(a) shows the tube orientation during SHG measurements in the transmission geometry, where the fundamental electric field was incident normal to the sample, and its polarization at an angle Ψ relative to the laboratory axis was rotated by a half wave plate from 0° to 180° . The SHG parallel (p polarization) and perpendicular (s polarization) polarizations with respect to the tube axis were measured using a linear polarizer. For selecting individual FI-FF and FF tubes, a long working distance microscope with a CCD camera was used.

Figures 4(c) and 4(d) show the SEM images of FI-FF and FF nanotubes, respectively, where the parameters of the tube size may be used for SHG comparison. The SHG intensity is known to increase with the tube diameter, as was observed in FF nanotubes.⁹ Figure 4(b) plots the SHG intensity for two varying FF nanotubes with diameters $8\ \mu\text{m}$ (circles) and $13\ \mu\text{m}$ (squares). To compare the SHG intensity of FI-FF with FF, we consider a FI-FF tube with a diameter approximately 3.5 times lower compared to the diameter of the FF tube.

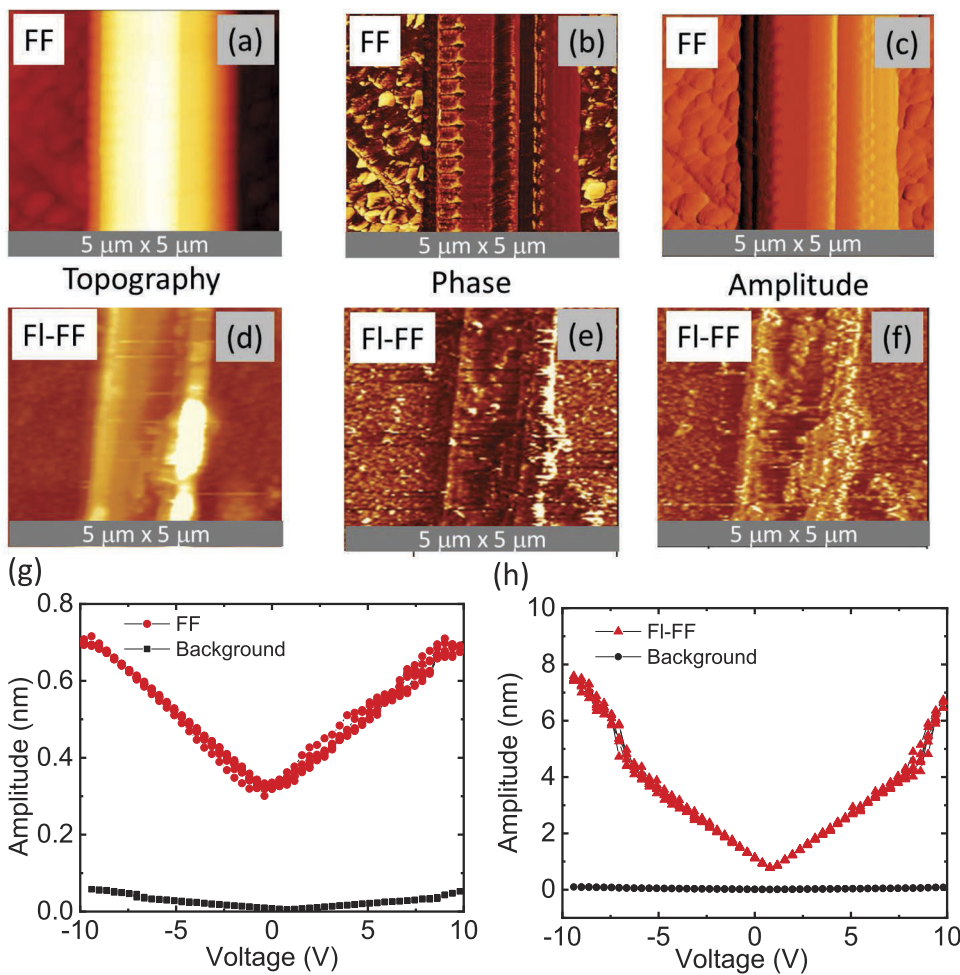


FIG. 3. Piezoforce microscopy images of FF (top row) and FI-FF (bottom row). [(a)–(c)] Topography, phase, and amplitude images of the FF nanotube. [(d)–(f)] Topography, phase, and amplitude images of the FI-FF nanotube. (g) Local amplitude piezoresponse loop from the FF nanotube. (h) Localized amplitude piezoresponse loop from the FI-FF nanotube.

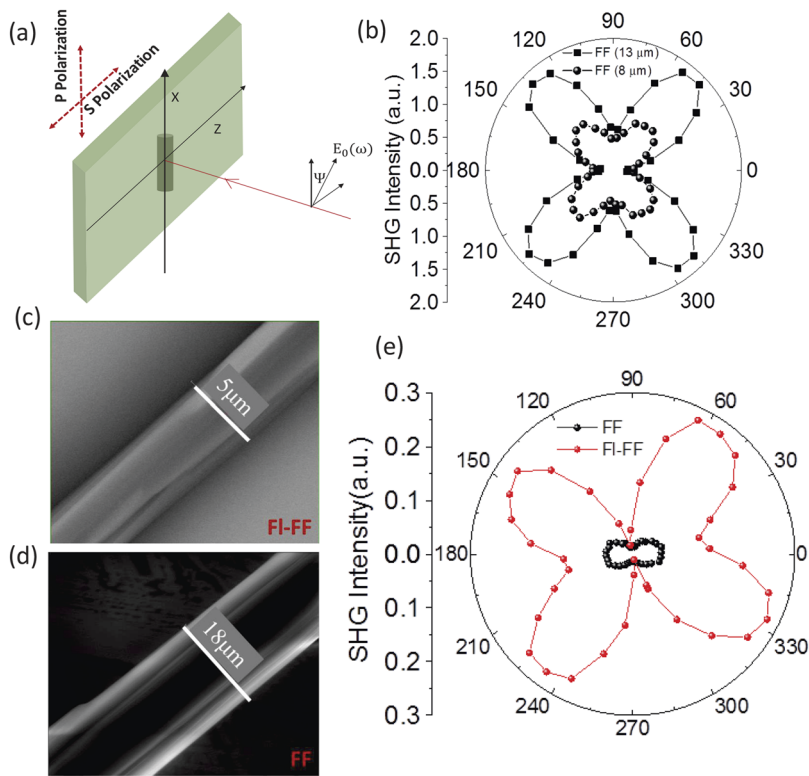


FIG. 4. (a) Orientation of the sample in the transmission SHG experiment. (b) Total SHG intensity from FF nanotubes with two different outer diameter nanotubes. The black square symbols correspond to a $13\ \mu\text{m}$ FF nanotube, and the black circular symbols correspond to an $8\ \mu\text{m}$ FF nanotube. (c) SEM image of the FI-FF nanotube and (d) SEM image of the FF nanotube used in the SHG experiment. (e) Total SHG intensity from FF (black circles) and FI-FF (red circles) nanotubes.

Figure 4(e) compares the SHG intensity (s polarization) between FF and FI-FF. The SHG intensity of the FI-FF (for a $5\ \mu\text{m}$ tube) is six times higher than the SHG intensity of the FF (for an $18\ \mu\text{m}$ tube). Scaling the SHG intensity to account for the difference in the tube diameter yields a factor of 20 by which the intensity of FI-FF is higher compared with FF. If we compare the p polarization (Fig. S3) data from FI-FF with FI-FF, we observe a different SHG polarimetry pattern. The p polarization data from the FI-FF nanotube has only two peaks as compared to the four peaks from FF nanotubes. This suggests that either FI-FF has a different symmetry compared to the $P6_1$ symmetry of FF nanotubes or has different nonlinear optical coefficients compared to FF. Determining the exact symmetry of FI-FF nanotubes is the subject of our future work. We discuss a few possible symmetry considerations based on the SHG signature of FI-FF in the [supplementary material](#).

We have also obtained SHG images from FF and FI-FF tubes using a microscope objective and a cooled CCD camera. The spot size of the fundamental beam is much smaller than the length of the nanotubes. Hence, the SHG is seen to originate only around the region of excitation and not from the entire tube. Figures 5(a) and 5(b) compare the bright-field image and the SHG image for the same tubes of the FI-FF sample. The SHG image was captured in 5 s; it clearly shows the edge of the tubes. In order to compare the SHG images from FF and FI-FF, we chose tubes of similar diameters. The bright-field and SHG images are superimposed in Figs. 5(c) and 5(d). The blue rectangle depicts the tube that was illuminated, and

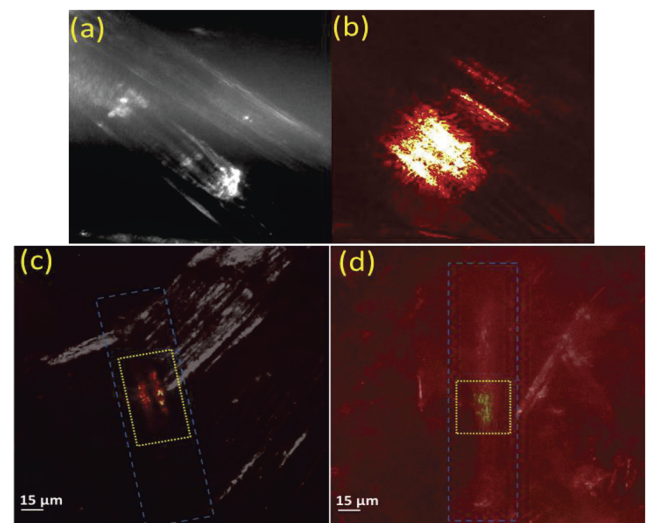


FIG. 5. (a) Bright-field image of FI-FF tubes. (b) SHG image from the same FI-FF tubes shown in (a). To compare the SHG intensity from FF and FI-FF tubes, we selected tubes of similar diameters. (c) and (d) show the SHG image superimposed on the bright-field image of FI-FF and FF tubes. The blue rectangle depicts the tube that was illuminated, and the yellow rectangle shows the SHG intensity. For the same laser power and geometry, the SHG images were obtained in 5 s for FI-FF (c) and in 60 s for FF in (d).

the yellow region shows the SHG intensity. The SHG image for FI-FF in Fig. 5(c) was obtained in 5 s compared to the SHG image of FF in Fig. 5(d), which is very weak and was obtained in 60 s. These SHG images are again a direct proof that FI-FF has a higher SHG efficiency compared to only FF.

In summary, fluorination of dipeptides that self-assemble into microstructures/nanostructures may have a significant impact in the area of nonlinear optics and piezoelectricity. The fluorinated FF dipeptide, FI-FF, which was synthesized by replacing H with F in the ortho position, self-assembles into tubular structures, similar to FF microtubes/nanotubes, opening up a path for probing nonlinear optical and piezoresponse properties. The piezoresponse coefficient (d_{15}) of a FI-FF tube of outer diameter close to 2 μm was found to be 600 pm/V. A similar diameter tube of FF yields a piezoresponse of only 50 pm/V. Similarly, SHG polarimetry from FI-FF tubes show at least 20 times higher intensity compared to FF nanotubes. Direct SHG images from FF and FI-FF tubes further provide evidence of a higher SHG efficiency for the fluorinated sample compared to only FF. DFT calculations were performed to find the minimum energy conformations of FI-FF. This work not only demonstrates the potential of fluorinated self-assembled biological nanostructures in enhancing nonlinear optical and piezoresponse properties but also provides a critical test for the future development of improved first principles approaches for guiding synthesis of such peptide molecules.

See the [supplementary material](#) for Synthesis, PFM, NMR spectra, and fitting of the SHG polarimetry data.

This research was supported in part by the U.S. National Science Foundation, Grant Nos. ECCS-1707588 (S.G.) and CHE-1665487 (R.G.). R.G. acknowledges the donors of the American Chemical Society Petroleum Research Fund (Grant No. PRF-53415-ND4) for partial support of this research. W.A.A. acknowledges the São Paulo Research Foundation (FAPESP Grant No. 2017/02317-2).

REFERENCES

- S. Roth and I. Freund, *J. Chem. Phys.* **70**(4), 1637–1643 (1979).
- R. M. Williams, W. R. Zipfel, and W. W. Webb, *Biophys. J.* **88**(2), 1377–1386 (2005).
- F. Tiaho, G. Recher, and D. Rouède, *Opt. Express* **15**(19), 12286–12295 (2007).
- C. H. Görbitz, *Chem. - Eur. J.* **13**(4), 1022–1031 (2007).
- A. Handelman, S. Lavrov, A. Kudryavtsev, A. Khatchaturiants, Y. Rosenberg, E. Mishina, and G. Rosenman, *Adv. Opt. Mater.* **1**(11), 875–884 (2013).
- Q. Li, H. Ma, A. Wang, Y. Jia, L. Dai, and J. Li, *Adv. Opt. Mater.* **3**(2), 194–198 (2015).
- Q. Li, Y. Jia, L. Dai, Y. Yang, and J. Li, *ACS Nano* **9**(3), 2689–2695 (2015).
- X. Yan, J. Li, and H. Möhwald, *Adv. Mater.* **23**(25), 2796–2801 (2011).
- S. Khanra, K. Ghosh, F. F. Ferreira, W. A. Alves, F. Punzo, P. Yu, and S. Guha, *Phys. Chem. Chem. Phys.* **19**(4), 3084–3093 (2017).
- N. Kol, L. Adler-Abramovich, D. Barlam, R. Z. Shneck, E. Gazit, and I. Rouso, *Nano Lett.* **5**(7), 1343–1346 (2005).
- J. Ryu and C. B. Park, *Biotechnol. Bioeng.* **105**(2), 221–230 (2010).
- A. Heredia, I. Bdkin, S. Kopyl, E. Mishina, S. Semin, A. Sigov, K. German, V. Bystrov, J. Gracio, and A. L. Kholkin, *J. Phys. D: Appl. Phys.* **43**(46), 462001 (2010).
- A. Handelman, B. Apter, N. Turko, and G. Rosenman, *Acta Biomater.* **30**, 72–77 (2016).
- J. George and K. G. Thomas, *J. Am. Chem. Soc.* **132**(8), 2502–2503 (2010).
- J. M. Slocik, A. O. Govorov, and R. R. Naik, *Nano Lett.* **11**(2), 701–705 (2011).
- S. Kogikoski, C. P. Sousa, M. S. Liberato, T. Andrade-Filho, T. Prieto, F. F. Ferreira, A. R. Rocha, S. Guha, and W. A. Alves, *Phys. Chem. Chem. Phys.* **18**(4), 3223–3233 (2016).
- C. P. Sousa, M. D. Coutinho-Neto, M. S. Liberato, L. T. Kubota, and W. A. Alves, *J. Phys. Chem. C* **119**(2), 1038–1046 (2015).
- B.-W. Park, R. Zheng, K.-A. Ko, B. D. Cameron, D.-Y. Yoon, and D.-S. Kim, *Biosens. Bioelectron.* **38**(1), 295–301 (2012).
- M. S. Liberato, S. Kogikoski, E. R. da Silva, D. R. de Araujo, S. Guha, and W. A. Alves, *J. Mater. Chem. B* **4**(8), 1405–1413 (2016).
- N. Even, L. Adler-Abramovich, L. Buzhansky, H. Dodiuk, and E. Gazit, *Small* **7**(8), 1007–1011 (2011).
- V. Nguyen, R. Zhu, K. Jenkins, and R. Yang, *Nat. Commun.* **7**, 13566 (2016).
- A. Levin, T. C. T. Michaels, L. Adler-Abramovich, T. O. Mason, T. Muller, B. Zhang, L. Mahadevan, E. Gazit, and T. P. J. Knowles, *Nat. Phys.* **12**(10), 926–930 (2016).
- S. Khanra, M. Abdullah-Al Mamun, F. F. Ferreira, K. Ghosh, and S. Guha, *ACS Appl. Nano Mater.* **1**(3), 1175–1187 (2018).
- S. Khanra, T. Cipriano, T. Lam, T. A. White, E. E. Fileti, W. A. Alves, and S. Guha, *Adv. Mater. Interfaces* **2**, 1500265–1500274 (2015).
- M. I. Souza, Y. M. Jaques, G. P. de Andrade, A. O. Ribeiro, E. R. da Silva, E. E. Fileti, É. d. S. Ávila, M. V. B. Pinheiro, K. Krambrock, and W. A. Alves, *J. Phys. Chem. B* **117**(9), 2605–2614 (2013).
- I. Bdkin, V. Bystrov, S. Kopyl, R. P. G. Lopes, I. Delgadillo, J. Gracio, E. Mishina, A. Sigov, and A. L. Kholkin, *Appl. Phys. Lett.* **100**(4), 043702 (2012).
- V. S. Bystrov, E. Seyedhosseini, S. Kopyl, I. K. Bdkin, and A. L. Kholkin, *J. Appl. Phys.* **116**(6), 066803 (2014).
- A. Handelman, P. Beker, N. Amdursky, and G. Rosenman, *Phys. Chem. Chem. Phys.* **14**(18), 6391–6408 (2012).
- A. Kholkin, N. Amdursky, I. Bdkin, E. Gazit, and G. Rosenman, *ACS Nano* **4**(2), 610–614 (2010).
- H. Kawai, *Jpn. J. Appl. Phys., Part 1* **8**(7), 975 (1969).
- R. G. Kepler and R. A. Anderson, *J. Appl. Phys.* **49**(3), 1232–1235 (1978).
- A. J. Lovinger, *Science* **220**(4602), 1115–1121 (1983).
- Q. M. Zhang, V. Bharti, and X. Zhao, *Science* **280**(5372), 2101–2104 (1998).
- C. H. Görbitz, *Chem. Commun.* **2006**(22), 2332–2334.
- R. F. Silva, D. R. Araujo, E. R. Silva, R. A. Ando, and W. A. Alves, *Langmuir* **29**(32), 10205–10212 (2013).
- T. Andrade-Filho, T. C. Martins, F. F. Ferreira, W. A. Alves, and A. R. Rocha, *Theor. Chem. Acc.* **135**(8), 185 (2016).
- C. J. Cramer, *Essential of Computational Chemistry* (John Wiley and Sons, 2004).
- A. V. Marenich, C. J. Cramer, and D. G. Truhlar, *J. Phys. Chem. B* **113**(18), 6378–6396 (2009).